ADVANCED OPTICAL MATERIALS
www.advopticalmat.de

Materials Views
www.MaterialsViews.com

CdS/ZnO Core/Shell Nanowire-Built Films for Enhanced Photodetecting and Optoelectronic Gas-Sensing Applications

Zheng Yang, Linjuan Guo, Baiyi Zu, Yanan Guo, Tao Xu, and Xincun Dou**

Uniform CdS/ZnO core/shell nanowires are hydrothermally synthesized using a two-step process and assembled into a photodetector and a NO_2 optoelectronic sensor for the first time. The corresponding photodetector exhibits a fast, reversible, and stable optoelectronic response with a rise time of ~26 ms, a decay time of ~2.1 ms and a stability of over 5 months. The remarkable photosensitivity and fast photoresponse are attributed to the formation of a heterojunction structure between CdS and ZnO, which greatly inhibits the recombination of photoinduced electrons and holes. The CdS/ZnO core/shell nanowires also show an excellent visible-light-activated gas sensing performance towards ppb-level NO_2 at room temperature. The responses range from 6.7% to 337% toward NO_2 concentrations of 5 to 1000 ppb. It is found that the sensitivity of the NO_2 sensor is dependent on the illuminated light intensity with a maximum value at 0.68 mW/cm^2. The sensing mechanisms of the CdS/ZnO nanowires under visible-light irradiation and the influence of light intensity are also discussed. The present CdS/ZnO core/shell nanowire not only benefits the fabrication of efficient photodetectors, but also makes the instant, optically controlled sensing of ppb-level NO_2 gas possible.

1. Introduction

One-dimensional heterojunction nanostructures consisting of two important functional materials have been extensively studied over recent years due to their great potential in improving semiconductor-based device technologies,[1–3] including nanowire or nanorod-based lasers,[4,5] photodetectors,[6–9] solar cells,[10,11] and gas sensors.[12–14] Core/shell nanowires that consist of two components with distinct functionality are ideal building blocks for nanoscale photodetectors and gas sensors since they have large surface-to-volume ratio, stable chemical and physical properties.[15–18] For photodetectors, the usually high electron-hole recombination rates can be greatly suppressed by the introduction of a core/shell nanowire structure,[19,20] resulting in an enhanced photocurrent. For gas sensors, one-dimensional heterojunction structures can enrich more versatile functions such as enhanced sensitivity,[13] lower operating temperature[21] and better selectivity[22] compared with single material.

CdS is an important II-VI compound semiconductor with a bandgap of ~2.4 eV and it has excellent optoelectronic properties in the visible-light region.[23–26] A variety of one-dimensional CdS nanostructures have been synthesized and fabricated into photodetectors with excellent performance in the visible-light region, such as large photocurrent to dark current ratio, short rise time and decay time.[27–29] Previously, it was proved that the photocurrent to dark current ratio of a CdS-based photodetector can be further enhanced through the formation of hetrojunctions.[30,31] As a result, it is considered that the construction of a continuous thin shell layer, whose band structure can facilitate efficient electron transfer from the CdS core to the shell, and subsequently sorting out electrons to preferentially transport in the shell layer and holes to transport in the core layer would be of great interest to develop highly efficient CdS-based photodetectors. ZnO, whose conduction band and valence band are 0.2 and 0.8 eV lower than those of CdS respectively,[32] can meet the requirements to construct a high performance CdS based photodetector. Furthermore, nanostructured ZnO, which is also an optoelectronic material,[5,33,34] is widely used as the sensing material to fabricate NO_2 gas sensors due to its outstanding sensing properties.[35–40] A core/shell nanowire structure with core and shell respectively functionalizes as the photodetecting

Z. Yang, L. J. Guo, Dr. B. Y. Zu, Dr. Y. N. Guo, Prof. X. C. Dou
Laboratory of Environmental Science and Technology
Xinjiang Technical Institute of Physics & Chemistry
Key Laboratory of Functional Materials and Devices for Special Environments
Chinese Academy of Sciences
Urumqi 830011, China
E-mail: byzu@ms.xjb.ac.cn; xcdou@ms.xjb.ac.cn
Z. Yang
University of the Chinese Academy of Sciences
Beijing 100049, China
T. Xu
Department of Chemistry and Biochemistry
Northern Illinois University
DeKalb, Illinois 60115, USA

DOI: 10.1002/adom.201400086

© 2014 WILEY-VCH Verlag GmbH & Co. KGaA, Weinheim

element and the gas sensing element will fascinate a unique gas sensor and shine light on optoelectronic gas sensing. As a result, the fabrication of CdS/ZnO core/shell nanowires can be a good choice to build photodetectors and the resulting NO_2 gas sensor would be of great importance to optoelectronically sense ppb-level NO_2 gas. Furthermore, the instant, optically-controlled sensing can be realized because the CdS/ZnO core/shell nanowires can combine both the advantages of photodetectors and gas sensors. However, there is no report on core/shell nanowires which simultaneously functionalize as a photodetector and an optoelectronic gas sensor.

Herein, CdS/ZnO core/shell nanowires were synthesized for the first time and were fabricated into a photodetector and a visible-light-activated NO_2 sensor. There are three crucial factors in this design to be highlighted. First, the formation of the core/shell heterojunction structure improves the photoinduced charge separation and thus leads to a great enhancement of the photocurrent compared to bare CdS nanowires. Second, the photoelectrons transferred from CdS core to the ZnO shell can promote the interaction between ZnO and NO_2, resulting in a remarkable enhancement of the room temperature NO_2 sensing properties activated by the visible-light illumination. Third, the thin thickness of the ZnO shell layer (<3 nm) brings NO_2 to the proximity of the CdS/ZnO interface. We show that the corresponding photodetector exhibits a fast, reversible, and stable optoelectronic response and the resulting NO_2 sensor makes the instant, optically-controlled sensing of ppb-level NO_2 gas possible.

2. Results and Discussion

2.1. Morphology Characterization of CdS/ZnO Core/Shell Nanowires

CdS/ZnO core/shell nanowires were synthesized using a two-step hydrothermal process. Firstly, uniform CdS nanowires were grown through a hydrothermal method from a reported method.[30] ZnO shell layer was then grown by the hydrothermal method and the shell thickness can be controlled through adjusting the concentration of precursors and the reaction temperature. X-ray diffraction (XRD) analysis was performed to investigate the crystal phase of CdS/ZnO core/shell nanowires (**Figure 1**a). It can be seen that for the CdS/ZnO core/shell nanowires, all the diffraction peaks can be well indexed as a mixture of hexagonal wurtzite CdS (JCPDS, 41–1049) and hexagonal wurtzite ZnO (JCPDS, 79–2205). The morphology of the CdS/ZnO core/shell nanowires was investigated by field emission scanning electron microscopy (FESEM) and high resolution transmission electron microscopy (HRTEM). Figure 1b shows the FESEM image of the CdS/ZnO core/shell nanowires, in which one can see that most of the CdS/ZnO core/shell nanowires have a diameter of 20–60 nm and length of several micrometers. To confirm the formation of the core/shell structure, HRTEM observation from the edge of an individual CdS nanowire and the interface of a CdS/ZnO core/shell nanowire was carried out, as shown in Figure 1c and d. From the comparison, one can see that the core part is the CdS nanowire and grows along the [001] direction, and the shell part is ZnO layer with an average thickness of 2~3 nm. It is considered

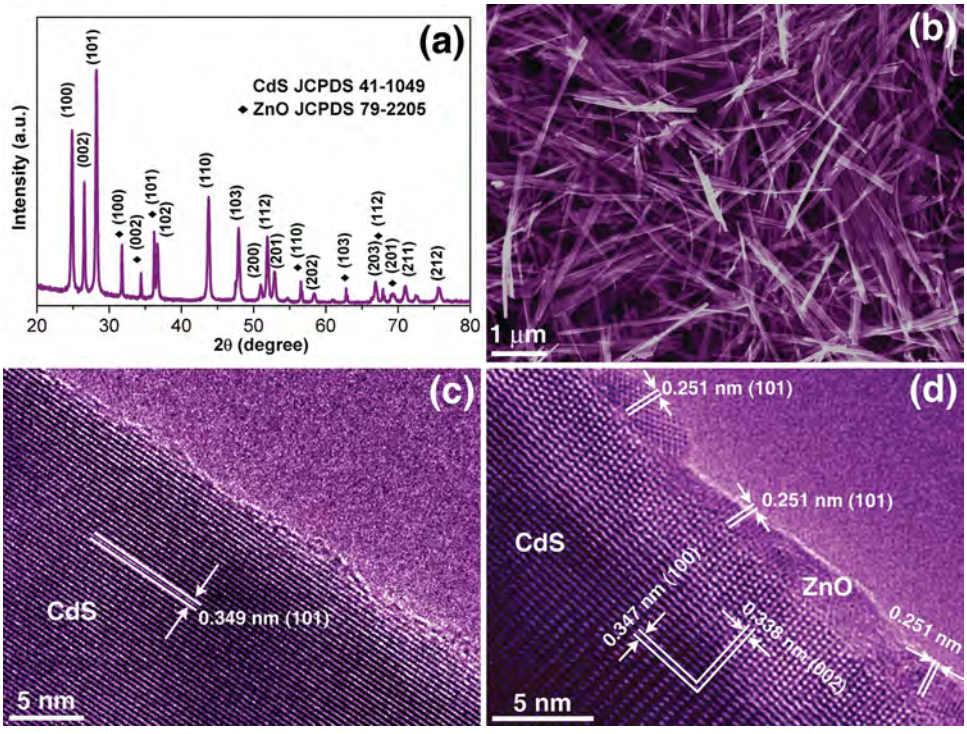

Figure 1. (a) XRD pattern, (b) FESEM image of the CdS/ZnO core/shell nanowires, HRTEM image of the edge of (c) a CdS nanowire and (d) a CdS/ZnO core/shell nanowire.

© 2014 WILEY-VCH Verlag GmbH & Co. KGaA, Weinheim

that in the second hydrothermal reaction process, the zinc ions adsorbed on the surface of CdS nanowires are hydrolyzed with the help of hexamine, leading to the formation of $Zn(OH)_2$. $Zn(OH)_2$ dehydrates into ZnO seeds under high temperature and pressure. With the growth time continuing, the ZnO shell layer forms.[41] It is expected that the present CdS/ZnO core/shell nanowires should show good photoresponse and gas sensing properties due to the desired heterojunction structure.

2.2. Photodetector Properties

The CdS/ZnO core/shell nanowires are constructed into a photodetector, as shown in **Figure 2**a, which shows the schematic diagram of the device for the optoelectronic properties evaluation. The SEM image of the brushed film is shown in Figure S1. The thickness of the film is confirmed to be 10 μm by SEM cross section observation. The current-voltage (I-V) characteristics of the photodetector, which were measured in dark condition and illuminated with 367 or 468 nm light (0.68 mW/cm^2) were shown in Figure 2b. Upon 468 nm light illumination, the current across the nanowire dramatically increases from 0 to 158 nA at an applied voltage of 4.0 V. The current further increases to 183 nA upon 367 nm light illumination at an applied voltage of 4.0 V. The increase of the photocurrent is ascribed to the effective separation of the photogenerated electron-hole pairs under illumination of which the energy of photons is larger than the band gap of either CdS or ZnO. Under 468

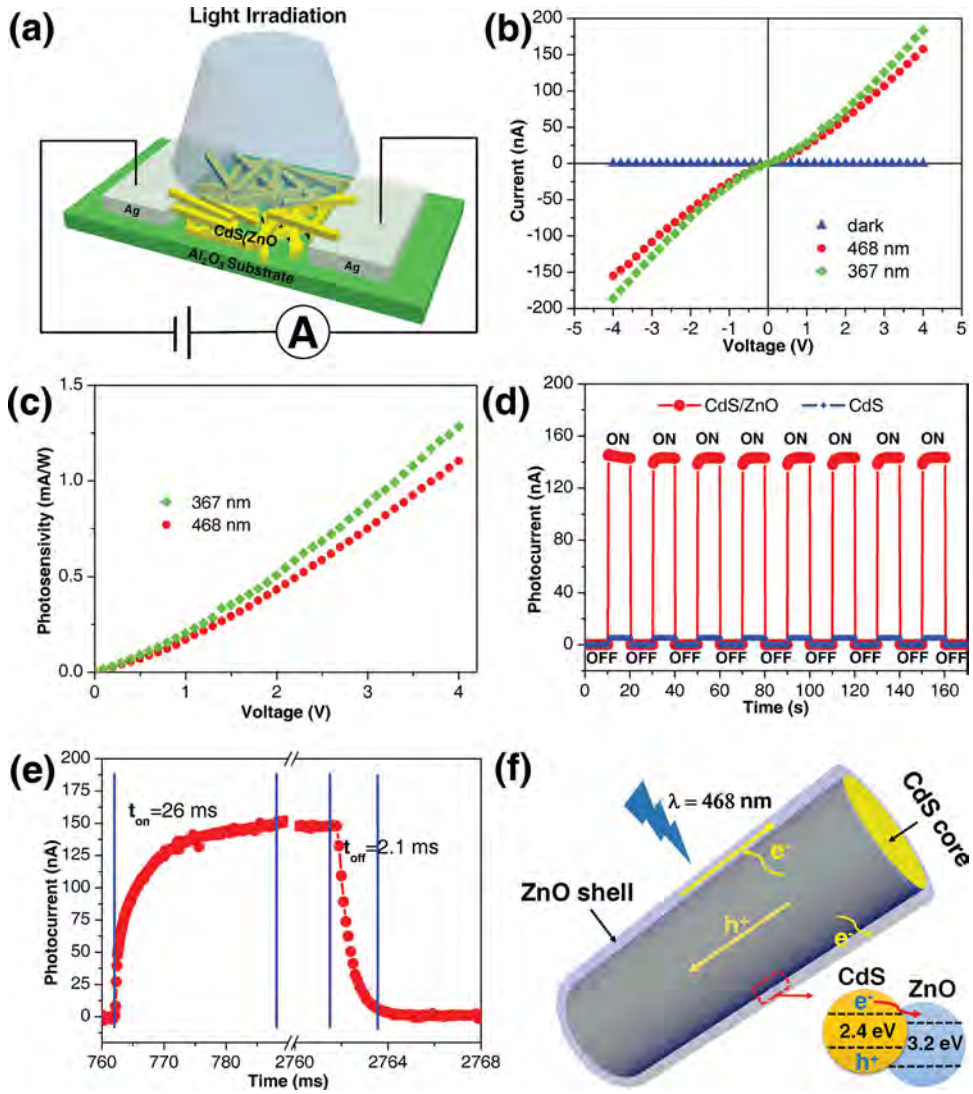

Figure 2. (a) Schematic diagram of a photodetector constructed from CdS/ZnO core/shell nanowires. (b) I–V characteristics of CdS/ZnO core/shell nanowire-based photodetector in dark condition and illuminated with 367 nm (0.68 mW/cm^2), 468 nm monochromatic light (0.68 mW/cm^2). (c) Photosensitivity calculated according to the I–V characteristics of the photodetector illuminated at 367 and 468 nm shown in Figure 2b. (d) Time-dependent photoresponse of the CdS/ZnO core/shell nanowire photodetector and a CdS nanowire photodetector measured by periodically turning on and off a 468 nm light (0.68 mW/cm^2) at a bias of 4 V. (e) Time-dependent photoresponse of a CdS/ZnO core/shell nanowire-based photodetector from light on (760–790 ms) to light off (2760–2768 ms) under 468 nm light (0.68 mW/cm^2) at a bias of 4 V. (f) Schematic diagram of the energy band structure, charge separation, transfer and transport in CdS/ZnO core/shell nanowires under 468 nm light illumination.

© 2014 WILEY-VCH Verlag GmbH & Co. KGaA, Weinheim

nm light, only CdS core nanowire can be excited. While under 367 nm light, both CdS core nanowire and ZnO shell layer will generate photoinduced electrons. Figure 2c shows photosensitivity calculated according to the *I–V* characteristics of the photodetector illuminated at 367 and 468 nm light shown in Figure 2b. At an applied bias of 4 V, the photosensitivities are 1.1 and 1.3 mA/W under 468 and 367 nm light illumination (0.68 mW/cm^2). Figure 2d shows the periodic photocurrent response of the CdS/ZnO core/shell nanowires and bare CdS nanowires under 468 nm light illumination (0.68 mW/cm^2) at room temperature and at an applied bias of 4 V. The light on and light off time are 10 s, respectively. For CdS/ZnO core/shell nanowires constructed photodetector, the photocurrent increases quickly from about zero (dark current) to 143 nA once light is on. The maximum photocurrent of each cycle is nearly the same and it almost unchanged once light is on, indicating a rather stable and reversible photoresponse. The photocurrent of CdS/ZnO core/shell nanowires-based photodetector is about 28 times larger than that of the pure CdS nanowires-based photodetector at a bias of 4 V. It should be noted that this dramatic improvement in photocurrent indicates that the recombination of photogenerated electrons was effectively inhibited due to the formation of the core/shell heterojunction structure. It is found that the photoresponse of the CdS/ZnO core/shell nanowire constructed photodetector can be optimized by changing the film thickness and 10 μm is found to be the most appropriate thickness (Figure S2). A closer examination of time responses (Figure 2e) shows that the fast photocurrent on-off process is consisted of photocurrent plateau and can be characterized by rise time (~26 ms) and decay time (~2.1 ms). The dark current is confirmed to be around 8.2 pA, as shown in Figure S3a. The decay time is always shorter than the rise time under different intensities of light illumination (Figure S3b–d). The shorter decay time was related to a fact that once the light was turned off, the number of photogenerated electrons and holes in the interface region decreased quickly. Compared to the CdS nanowire-based photodetector in Figure 2d and other CdS nanostructure-based photodetectors (listed in Table S1),[23,25,27,42] the present CdS/ZnO core/shell nanowire-based photodetector shows a superior photocurrent to dark current ratio since the dark current is zero evaluated by our measuremental setup. Compared to the ZnO nanostructure or hybrid-based photodetectors,[43–46] the present CdS/ZnO core/shell nanowire-based photodetector shows not only a remarkable photocurrent to dark current ratio, but also a much shorter rise time and decay time. It is also found that the photoresponse of the present CdS/ZnO core/shell nanowire-based photodetector is much better than that of the CdS and ZnO nanowire (SEM image shown in Figure S4) mixture constructed photodetector (Figure S5), indicating the superiority of the core/shell structure in photodetecting application. The shell thickness also influences the photoresponse and a thick shell (~10 nm, SEM image shown in Figure S6) would lead to a decrease of the photocurrent to dark current ratio (Figure S7).

As schematically shown in Figure 2f, when the CdS/ZnO core/shell nanowires are under the illumination of visible-light, photogenerated electrons are injected from the conduction band of CdS into the conduction band of ZnO, leading to a high density of electrons in the conduction band of ZnO.[6] The holes transport along CdS nanowires, while the electrons move along ZnO shell. As a result, the heterojunction structure between CdS and ZnO can retard the recombination probability of excess carriers and prolong lifetime of the photogenerated excess carriers, leading to a remarkable photocurrent improvement.

2.3. Optoelectronic Gas Sensor Properties

To evaluate the NO_2 sensing performance of the CdS/ZnO core/shell nanowires constructed optoelectronic sensor, independent resistance change measurements are carried out at 8 different concentrations of NO_2 ranging from 5 ppb to 1 ppm. **Figure 3**a shows the responses of a CdS/ZnO core/shell nanowires–based optoelectronic gas sensor upon exposure to 8 different concentrations of NO_2 gas under 468 nm light illumination (0.68 mW/cm^2) at room temperature and at a bias of 4.5 V. The thickness of the film is 10 μm. The relative sensor response in resistance is defined as Equation (1),

$$\text{Response} = \left(R_g - R_a\right) / R_a \times 100\% \quad (1)$$

where R_g and R_a are the electrical resistances of the sensors in NO_2 gas or in air measured under the same light intensity, respectively. One can see that the sensor resistance increases quickly once NO_2 gas is introduced and the response gradually saturates. Upon purging with air, the sensor resistance decreases to the intial value due to the desorption of NO_2 molecules from the surface of ZnO shell, which leads to the release of the attracted photogenerated electrons by NO_2 molecules. The CdS/ZnO core/shell nanowires-based gas sensor shows responses ranging from 6.7% to 337% by varying the NO_2 concentration from 5 ppb to 1 ppm. The detection limit of the present sensor is measured to be 5 ppb.

Figure 3b plots the responses of CdS/ZnO core/shell nanowires-based optoelectronic gas sensor as a function of NO_2 concentrations. The data points can be well fitted with Langmuir isotherm adsorption, as shown in Equation (2),

$$\text{Response} = 446.43 / \left(1 + 326.93 / C\right) \quad (2)$$

where C represents concentration of NO_2. It can also be further confirmed by the linear fitting of Response^{-1} versus C^{-1}, as shown in the inset of Figure 3b. The results can be understood as the surface coverage of adsorbed NO_2 molecules follows Langmuir isotherm adsorption.[47] At lower concentrations, the NO_2 sensor exhibits an approximate linear relation between the sensor response and the NO_2 concentration because the surface adsorption sites are not saturated. At higher concentrations, the surface coverage tends to saturate and hence leads to the saturation response.[48] Figure 3c presents the response time and recovery time which are calculated by 90% of the total time of the resistance change takes upon different concentrations of NO_2, as shown in Equation (3) and Equation (4),

$$\text{Response time} = t_{90\%\,\max} - t_{\text{initial}} \quad (3)$$

© 2014 WILEY-VCH Verlag GmbH & Co. KGaA, Weinheim

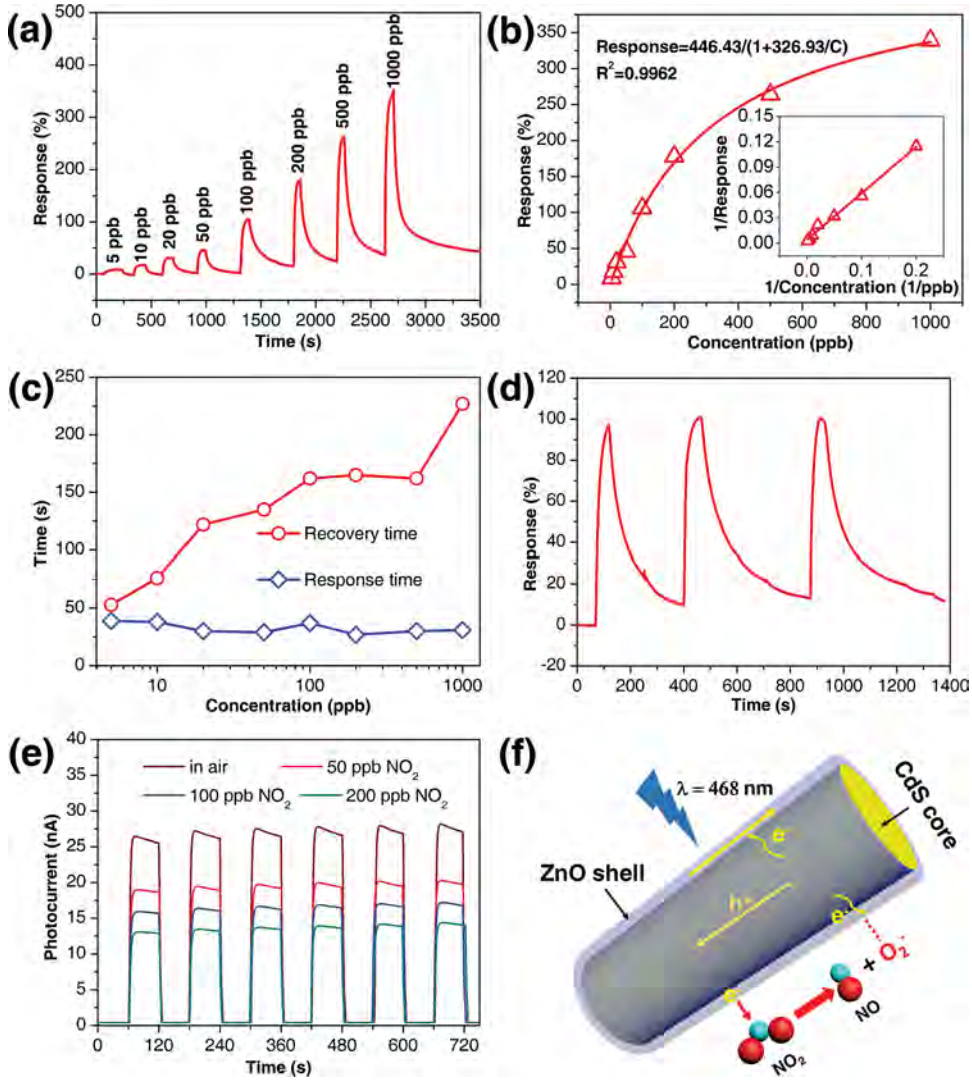

Figure 3. (a) Plot of response *versus* time for a CdS/ZnO core/shell nanowire-based sensor upon exposure to NO_2 gas with concentrations ranging from 5 to 1000 ppb at room temperature (under illumination of 468 nm monochromatic light, 0.68 mW/cm^2). (b) Normalized response versus NO_2 concentrations fitted using Langmuir isotherm adsorption. Inset: 1/Response versus 1/C with linear line fitting. (c) Response time and recovery time calculated by 90% of the total time of the resistance change upon different concentrations of NO_2. (d) Response changes of a sensor during 3 successive cycles of exposure to 100 ppb NO_2. (e) Time dependent photoresponse in air or in NO_2 with a concentration of 50, 100, 200 ppb by periodically tuning on and off a 468 nm monochromatic light (0.68 mW/cm^2). (f) Light enhanced NO_2 sensing mechanisms in CdS/ZnO core/shell nanowires-based optoelectronic NO_2 gas sensor.

$$\text{Recovery time} = t_{10\%\,\max} - t_{\max} \quad (4)$$

where $t_{90\%\ \max}$ is the time point when resistance reached 90% of the maxium value after NO_2 is introduced, t_{initial} is the time point when the NO_2 gas is introduced, $t_{\max}$ is the time point when the resistance in NO_2 reaches the maxium value, $t_{10\%\ \max}$ is the time point when resistance reached 10% of the maximum value after air is purged.[49] The response time keeps in the range of 27–40 s, while the recovery time increases from 53 s to 227 s with the increase of the NO_2 concentration. Compared to some of the other recently explored hetrojunction-based room temperature NO_2 gas sensors (listed in Table S2),[13,50–56] our CdS/ZnO core/shell nanowires-based optoelectronic NO_2 gas sensor displays a greater than an order of magnitude faster response time and recovery time than the reported values. Furthermore, the detection limit (5 ppb) of our NO_2 sensor is much higher than the reported values. In order to confirm the repeatability of the present optoelectronic NO_2 gas sensor, the sensor was exposed to 100 ppb NO_2 for three successive cycles (Figure 3d). The response of each cycle keeps nearly at the same value and they all agree well with the fitting in Figure 3b, indicating the excellent repeatability of our CdS/ZnO core/shell nanowire-based optoelectronic NO_2 sensors. Time dependent photoresponse of the sensor in air or in NO_2 was tested by periodically tuning on and off a 468 nm monochromatic light (0.68 mW/cm^2), as shown in Figure 3e. It is clearly shown that the sensor can work once light is illuminated and it is repeatable. The optoelectronic properties of the CdS/ZnO core/shell nanowires make the instant, optically-controlled sensing of NO_2 possible since the photoresponse is fast and it takes

© 2014 WILEY-VCH Verlag GmbH & Co. KGaA, Weinheim

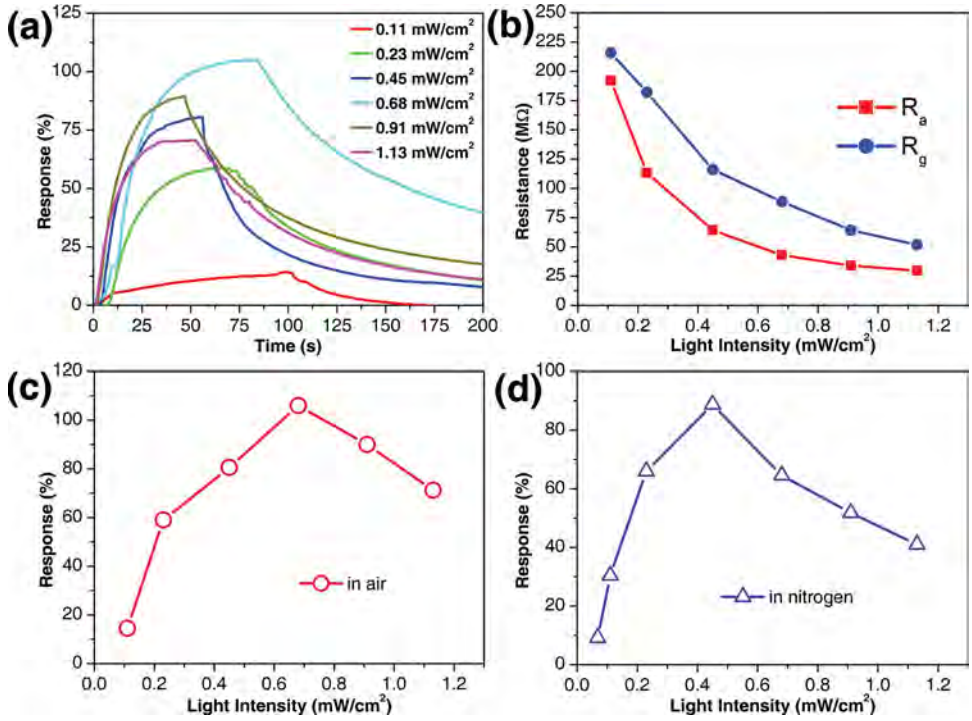

Figure 4. (a) Room temperature response curve of the CdS/ZnO core/shell nanowires-based optoelectronic NO_2 gas sensor in air at a NO_2 concentration of 100 ppb when the light intensity varies from 0.11 mW/cm^2 to 1.13 mW/cm^2. (b) Light intensity dependent resistance in air (R_a) and in 100 ppb NO_2 (R_g) at room temperature. (c) The corresponding response plot in air *versus* light intensity at room temperature. (d) The response plot in nitrogen *versus* light intensity at room temperature.

only tens of milliseconds for the photocurrent to be stable and always be the same level. A sensor with larger film thickness (Figure S8) or with thick shell (Figure S9) would lead to a decrease in the sensor response to NO_2. The sensor response towards NO_2 of the CdS and ZnO nanowire mixture constructed sensor is even worse (Figure S10), indicating the superiority of the core/shell structure in gas sensing application.

Comparing with the pristine CdS nanowires, the remarkable improvement in the response of the CdS/ZnO core/shell nanowires to NO_2 under light illumination can be explained by the modulation of photo-induced charge transfer at the CdS/ZnO heterojunction. When a CdS/ZnO core/shell nanowire is exposed to air and under visible-light illumination, ionic species, such as O^-, O^{2-} always form on the surface of ZnO above 200 °C, while O_2^- usually form beneath 200 °C due to photoelectron transfer from ZnO to the adsorbed oxygen molecules,[57] which leads to the formation of an electron-depletion layer (comparable to the Dybe length of ZnO, ~30 nm[57] in the surface region of the ZnO shell. As a result, this surface electron-depletion layer of the ZnO shell overlaps the depletion region in the vicinity of the core/shell interface since the average thickness of the ZnO shell is less than 3 nm.

When a CdS/ZnO core/shell nanowire is exposed to NO_2 and under visible-light illumination (schematically shown in Figure 3f), the adsorbed NO_2 gas molecules (NO_2(g)) will capture photoelectrons directly from ZnO shell and form NO specie according to Equation (5).[58]

$$NO_2(g) + e^- \rightarrow 2NO + O_2^-(ads) \quad (5)$$

As a result, the surface electron-depletion layer expands and results in the increase of the overall resistance when exposed to NO_2 gas. Under light illumination, a high density of electrons accumulates in the conduction band of ZnO due to the efficient restraining of photogenerated electrons go back to CdS core. Thus, more electrons in ZnO shell participate in the reaction with NO_2 gas molecules and a remarkable improvement in the gas sensing performance is achieved.

2.4. Influence of Light Intensity on Gas Sensing Properties

As an optoelectronic gas sensor, the influence of the light intensity on gas sensing properties needs to be investigated. Despite of some handful reports on the light enhanced gas sensors, the influence of the light intensity on sensing performance is not extensively studied.[59] **Figure 4**a shows the dynamic responses of a CdS/ZnO core/shell nanowires-based gas sensor to 100 ppb NO_2 gas at room temperature under 468 nm light illumination at different light intensities from 0.11 mW/cm^2 to 1.13 mW/cm^2. It should be noted that the sensor response in dark can not be evaluated due to the measurement setup limit. As shown in Figure 4b, the resistance in air (R_a) or in NO_2 (R_g) under light illumination tends to saturate with the increase of light intensity. In other words, the photocurrent tends to saturate with the increase of light

© 2014 WILEY-VCH Verlag GmbH & Co. KGaA, Weinheim

intensity and would limit the quantity of photogenerated electrons participate in the reaction with adsorbed NO_2. The response plot of the CdS/ZnO core/shell nanowires-based NO_2 gas sensor *versus* the change of the light intensity is shown in Figure 4c. It is obvious that the sensor response firstly increases from 14.5% to 106% with the increase of light intensity, and then decreases from 106% to 71.3%. The light intensity value of 0.68 mW/cm^2 acts as a shift point. To further confirm that the response change on light intensity is induced by NO_2 rather than O_2, the sensor is also tested using nitrogen as the carrier gas, as shown in Figure S11. The sensor response is shown in Figure 4d, in which one can see that there is a similiar light intensity dependent response change with the maximum response at 0.45 mW/cm^2. The sensor response plot in air *versus* light intensity at 50 °C towards 50 ppb NO_2 also shows a shift point at 0.068 mW/cm^2 (Figure S12). These results strongly emphasized that the influence of light intensity on the sensor response is remarkable. There is a best light intensity value to obtain the highest sensor response, which is totally different from the previously reported results.[13,60] The present observation makes the sensor behavior be controllable by adjusting the illuminated light intensity.

It is reported that ultraviolet light irradiation was used during the recovery of the NO_2 gas sensor to reduce the desorption energy level of the NO_2 gas.[61–63] Here, we assume that the visible-light illumination in our work has the similar effect since the wavelength of our light is 468 nm. With the increase of light intensity, desorption becomes much more easily. There is a balance between light enhanced gas sensing and light induced gas desorption. As a result, one should pay special attention to control the illuminated light intensity in order to get an optimized sensing performance.

3. Conclusion

CdS/ZnO core/shell nanowires have been synthesized using a two-step hydrothermal process. The CdS/ZnO core/shell nanowires are constructed into a photodetector and its resulting photocurrent is ~28 times greater than that of the pure CdS nanowires-based photodetector at at the same bias. The dramatic improvement in photocurrent indicates the recombination of photogenerated electrons is effectively inhibited due to the formation of the core/shell heterojunction structure. The rise time of the device is of ~26 ms and the decay time is of ~2.1 ms. The responses ranged from 6.7% to 337% toward NO_2 concentrations of 5 to 1000 ppb when applied as a room temperature optoelectronic gas sensor. The remarkable improvement in the gas sensing performance under light illumination is attributed to the huge increase in photoelectrons density in ZnO shell, thus the number of electrons that participate in the reaction with NO_2 gas molecules greatly increases. The sensitivity of the optoelectronic NO_2 was dependent on the illuminated light intensity due to a balance between light enhanced optoelectronic gas sensing and light induced gas desorption. The present results will shine light on both nanostructured photodetectors and optoelectronic sensing of hazardous gases.

4. Experimental Section

Synthesis of CdS/ZnO Core/Shell Nanowires: Cadmium nitrate, thiourea, ethylenediamine, zinc acetate and hexamine are all analytical grade and were bought from Sinopharm Chemical Reagent Co. Ltd.

CdS/ZnO core/shell nanowires were synthesized using a two-step hydrothermal process. Firstly, uniform CdS nanowires were grown through a hydrothermal method from a reported method.[30] In brief, cadmium nitrate (1.9 g) and thiourea (1.42 g) were added into a teflon stainless steel autoclave that had been filled with ethylenediamine to 60% of its capacity (50 mL). The autoclave was maintained at 180 °C for 48 h and allowed to cool down to room temperature. A yellow precipitate (CdS nanowires) was filtered and washed several times with absolute ethanol and deionized water to remove the residue of organic solvent. Secondly, CdS nanowires (0.175 g) were put into deionized water (30 mL) and ultrasonic treated for 20 min. Then, zinc acetate (0.133 g) and hexamine (0.085 g) were added into the mixture above. After 10 min magnetic stirring, the mixture was sealed in a teflon stainless autoclave of 50 mL capacity, and kept at 120 °C for 12 h and allowed to cool down to room temperature. The final products were filtered, washed several times with absolute ethanol and deionized water, and dried in vacuum at 65 °C for 6 h.

Characterization of CdS/ZnO Core/Shell Nanowires: X-ray diffraction (XRD) measurement was carried out using powder XRD (Bruker D8 Advance, with Cu-Kα radiation operating at 40 kV and 40 mA, scanning from 2θ = 10 to 90°). Field-emission scanning electron microscopy (FESEM, ZEISS SUPRA 55VP) and transmission electron microscope (JEM-2011 TEM, 200 kV) were used to characterize the morphology of the samples.

Device Fabrication, Optoelectronic Properties and Gas Sensing Properties Testing: Initially, the CdS/ZnO core/shell nanowires were mixed with deionized water in a weight ratio of 100:25 and ground in a mortar for 15 min to form a paste. The paste was then coated on a ceramic substrate by a thin brush to form a sensing film on which silver interdigitated electrodes with both finger-width and inter-finger spacing of about 200 μm was previously printed. The thickness of the film was controlled by the brushed cycles. The sample was dried naturally in air overnight. The photoelectric response and I-V curves were recorded by Controlled Intensity Modulated Photocurrent Spectrometer 70 (CIMPS-2, ZAHNER) system under 367 or 468 nm monochromatic light. The measurement was conducted in a conventional two-electrode configuration. Gas sensing properties were measured by a CGS-1TP (Chemical Gas Sensor-1 Temperature Pressure) intelligent gas sensing analysis system (Beijing Elite Tech Co., Ltd., China) with 468 nm monochromatic light illumination. The sensors were pre-heated at room temperature for about 24 h. The required amount of gas was injected into the chamber (14 mL) using a 1 ml syringe and was mixed with air (relative humidity was about 25%) or nitrogen. After the sensor resistances reached a new constant value, air was purged in to recover the sensor.

Supporting Information

Supporting Information is available from the Wiley Online Library or from the author.

Acknowledgements

We thank Prof. Xiaosheng Fang in Fudan University for helpful discussions. Financial supports by the National Natural Science Foundation of China (51372273, 51201180, 21204100), the "One Hundred Talents" program of Chinese Academy of Sciences (Y12H981601), the "Western Light" program of Chinese Academy of Sciences (LHXZ201102), the International Scientific Cooperation Program of Xinjiang (20136008), the "Xinjiang Science Foundation for

© 2014 WILEY-VCH Verlag GmbH & Co. KGaA, Weinheim

Distinguished Young Scholars" (2013711015) and SRF for ROCS, SEM are gratefully acknowledged.

Received: February 19, 2014
Revised: April 29, 2014
Published online: May 20, 2014

[1] L. J. Lauhon, M. S. Gudiksen, D. Wang, C. M. Lieber, *Nature* **2002**, *420*, 57–61.
[2] M. S. Gudiksen, L. J. Lauhon, J. Wang, D. C. Smith, C. M. Lieber, *Nature* **2002**, *415*, 617–620.
[3] U. K. Gautam, X. Fang, Y. Bando, J. Zhan, D. Golberg, *ACS Nano* **2008**, *2*, 1015–1021.
[4] F. Qian, Y. Li, S. Gradečak, H.-G. Park, Y. Dong, Y. Ding, Z. L. Wang, C. M. Lieber, *Nat. Mater.* **2008**, *7*, 701–706.
[5] J. Huang, S. Chu, J. Kong, L. Zhang, C. M. Schwarz, G. Wang, L. Chernyak, Z. Chen, J. Liu, *Adv. Opt. Mater.* **2013**, *1*, 179–185.
[6] F. Zhang, Y. Ding, Y. Zhang, X. Zhang, Z. L. Wang, *ACS Nano* **2012**, *6*, 9229–9236.
[7] B. Tian, X. Zheng, T. J. Kempa, Y. Fang, N. Yu, G. Yu, J. Huang, C. M. Lieber, *Nature* **2007**, *449*, 885–889.
[8] Q. Yang, X. Guo, W. Wang, Y. Zhang, S. Xu, D. H. Lien, Z. L. Wang, *ACS Nano* **2010**, *4*, 6285–6291.
[9] F. Zhang, S. Niu, W. Guo, G. Zhu, Y. Liu, X. Zhang, Z. L. Wang, *ACS Nano* **2013**, *7*, 4537–4544.
[10] S. L. Howell, S. Padalkar, K. Yoon, Q. Li, D. D. Koleske, J. J. Wierer, G. T. Wang, L. J. Lauhon, *Nano Lett.* **2013**, *13*, 5123–5128.
[11] S.-K. Kim, R. W. Day, J. F. Cahoon, T. J. Kempa, K.-D. Song, H.-G. Park, C. M. Lieber, *Nano Lett.* **2012**, *12*, 4971–4976.
[12] H. Huang, H. Gong, C. L. Chow, J. Guo, T. J. White, M. S. Tse, O. K. Tan, *Adv. Funct. Mater.* **2011**, *21*, 2680–2686.
[13] S. Park, S. An, Y. Mun, C. Lee, *ACS Appl. Mater. Interfaces* **2013**, *5*, 4285–4292.
[14] F. Gu, H. Zeng, Y. B. Zhu, Q. Yang, L. K. Ang, S. Zhuang, *Adv. Opt. Mater.* **2014**, *2*, 189–196.
[15] G. Shen, P.-C. Chen, K. Ryu, C. Zhou, *J. Mater. Chem.* **2009**, *19*, 828–839.
[16] T. Zhai, L. Li, X. Wang, X. Fang, Y. Bando, D. Golberg, *Adv. Funct. Mater.* **2010**, *20*, 4233–4248.
[17] Y. Xia, P. Yang, Y. Sun, Y. Wu, B. Mayers, B. Gates, Y. Yin, F. Kim, H. Yan, *Adv. Mater.* **2003**, *15*, 353–389.
[18] R. Yan, D. Gargas, P. Yang, *Nat. Photonics* **2009**, *3*, 569–576.
[19] D. Rudolph, S. Funk, M. Döblinger, S. Morkötter, S. Hertenberger, L. Schweickert, J. Becker, S. Matich, M. Bichler, D. Spirkoska, I. Zardo, J. J. Finley, G. Abstreiter, G. Koblmüller, *Nano Lett.* **2013**, *13*, 1522–1527.
[20] J. Xiang, W. Lu, Y. Hu, Y. Wu, H. Yan, C. M. Lieber, *Nature* **2006**, *441*, 489–493.
[21] P. A. Russo, N. Donato, S. G. Leonardi, S. Baek, D. E. Conte, G. Neri, N. Pinna, *Angew. Chem.- Int. Edit.* **2012**, *51*, 11053–11057.
[22] G. Aluri, A. Motayed, A. Davydov, V. Oleshko, K. Bertness, M. Rao, *IEEE Sens. J.* **2013**, *13*, 1883–1888.
[23] Y. Wang, G. Chen, M. Yang, G. Silber, S. Xing, L. H. Tan, F. Wang, Y. Feng, X. Liu, S. Li, H. Chen, *Nat. Commun.* **2010**, *1*, 87.
[24] D. Wu, Y. Jiang, Y. Zhang, Y. Yu, Z. Zhu, X. Lan, F. Li, C. Wu, L. Wang, L. Luo, *J. Mater. Chem.* **2012**, *22*, 23272–23276.
[25] Y. Ye, L. Dai, X. Wen, P. Wu, R. Pen, G. Qin, *ACS Appl. Mater. Interfaces* **2010**, *2*, 2724–2727.
[26] K. Heo, H. Lee, Y. Park, J. Park, H.-J. Lim, D. Yoon, C. Lee, M. Kim, H. Cheong, J. Park, *J. Mater. Chem.* **2012**, *22*, 2173–2179.
[27] T.-Y. Wei, C.-T. Huang, B. J. Hansen, Y.-F. Lin, L.-J. Chen, S.-Y. Lu, Z. L. Wang, *Appl. Phys. Lett.* **2010**, *96*, 013508.
[28] J. Jie, W. Zhang, Y. Jiang, X. Meng, Y. Li, S. Lee, *Nano Lett.* **2006**, *6*, 1887–1892.
[29] Q. Li, R. M. Penner, *Nano Lett.* **2005**, *5*, 1720–1725.
[30] J. Zhai, L. Wang, D. Wang, H. Li, Y. Zhang, D. q. He, T. Xie, *ACS Appl. Mater. Interfaces* **2011**, *3*, 2253–2258.
[31] H. Lin, H. Liu, X. Qian, S.-W. Lai, Y. Li, N. Chen, C. Ouyang, C.-M. Che, Y. Li, *Inorg. Chem.* **2011**, *50*, 7749–7753.
[32] Y. Xu, M. A. Schoonen, *Am. Mineral.* **2000**, *85*, 543–556.
[33] J. Song, S. A. Kulinich, J. Yan, Z. Li, J. He, C. Kan, H. Zeng, *Adv. Mater.* **2013**, *25*, 5750–5755.
[34] H. Zeng, G. Duan, Y. Li, S. Yang, X. Xu, W. Cai, *Adv. Funct. Mater.* **2010**, *20*, 561–572.
[35] M. Chen, Z. Wang, D. Han, F. Gu, G. Guo, *J. Phys. Chem. C* **2011**, *115*, 12763–12773.
[36] S. Bai, J. Hu, D. Li, R. Luo, A. Chen, C. C. Liu, *J. Mater. Chem.* **2011**, *21*, 12288–12294.
[37] Z. Jing, J. Zhan, *Adv. Mater.* **2008**, *20*, 4547–4551.
[38] X. Pan, X. Liu, A. Bermak, Z. Fan, *ACS Nano* **2013**, *7*, 9318–9324.
[39] A. M. Andringa, J. R. Meijboom, E. C. Smits, S. G. Mathijssen, P. W. Blom, D. M. De Leeuw, *Adv. Funct. Mater.* **2011**, *21*, 100–107.
[40] L. Wang, Z. Lou, T. Fei, T. Zhang, *J. Mater. Chem.* **2012**, *22*, 4767–4771.
[41] S. Xu, Z. Wang, *Nano Res.* **2011**, *4*, 1013–1098.
[42] H. Lee, K. Heo, A. Maaroof, Y. Park, S. Noh, J. Park, J. Jian, C. Lee, M. J. Seong, S. Hong, *Small* **2012**, *8*, 1650–1656.
[43] A. Manekkathodi, Y.-J. Wu, L.-W. Chu, S. Gwo, L.-J. Chou, L.-J. Chen, *Nanoscale* **2013**, *5*, 12185–12191.
[44] W. Tian, T. Zhai, C. Zhang, S. L. Li, X. Wang, F. Liu, D. Liu, X. Cai, K. Tsukagoshi, D. Golberg, *Adv. Mater.* **2013**, *25*, 4625–4630.
[45] L. Hu, M. Chen, W. Shan, T. Zhan, M. Liao, X. Fang, X. Hu, L. Wu, *Adv. Mater.* **2012**, *24*, 5872–5877.
[46] L. Hu, J. Yan, M. Liao, H. Xiang, X. Gong, L. Zhang, X. Fang, *Adv. Mater.* **2012**, *24*, 2305–2309.
[47] D. Zhang, Z. Liu, C. Li, T. Tang, X. Liu, S. Han, B. Lei, C. Zhou, *Nano Lett.* **2004**, *4*, 1919–1924.
[48] P. C. Chen, S. Sukcharoenchoke, K. Ryu, L. Gomez de Arco, A. Badmaev, C. Wang, C. Zhou, *Adv. Mater.* **2010**, *22*, 1900–1904.
[49] F. Favier, E. C. Walter, M. P. Zach, T. Benter, R. M. Penner, *Science* **2001**, *293*, 2227–2231.
[50] W. Yuan, A. Liu, L. Huang, C. Li, G. Shi, *Adv. Mater.* **2012**, *25*, 766–771.
[51] S. Ji, H. Wang, T. Wang, D. Yan, *Adv. Mater.* **2013**, *25*, 1755–1760.
[52] S. Deng, V. Tjoa, H. M. Fan, H. R. Tan, D. C. Sayle, M. Olivo, S. Mhaisalkar, J. Wei, C. H. Sow, *J. Am. Chem. Soc.* **2012**, *134*, 4905–4917.
[53] A. Sharma, M. Tomar, V. Gupta, *J. Mater. Chem.* **2012**, *22*, 23608–23616.
[54] S. Ammu, V. Dua, S. R. Agnihotra, S. P. Surwade, A. Phulgirkar, S. Patel, S. K. Manohar, *J. Am. Chem. Soc.* **2012**, *134*, 4553–4556.
[55] S. Cui, Z. Wen, E. C. Mattson, S. Mao, J. Chang, M. Weinert, C. J. Hirschmugl, M. Gajdardziska-Josifovska, J. Chen, *J. Mater. Chem. A* **2013**, *1*, 4462–4467.
[56] G. Lu, L. E. Ocola, J. Chen, *Adv. Mater.* **2009**, *21*, 2487–2491.
[57] N. Barsan, U. Weimar, *J. Electroceram.* **2001**, *7*, 143–167.
[58] S.-W. Fan, A. K. Srivastava, V. P. Dravid, *Appl. Phys. Lett.* **2009**, *95*, 142106.
[59] B. de Lacy Costello, R. Ewen, N. M. Ratcliffe, M. Richards, *Sens. Actuat. B* **2008**, *134*, 945–952.
[60] S. Mishra, C. Ghanshyam, N. Ram, R. Bajpai, R. Bedi, *Sens. Actuat. B* **2004**, *97*, 387–390.
[61] J. Lee, O. S. Kwon, D. H. Shin, J. Jang, *J. Mater. Chem. A* **2013**, *1*, 9099–9106.
[62] G. Lu, S. Park, K. Yu, R. S. Ruoff, L. E. Ocola, D. Rosenmann, J. Chen, *ACS Nano* **2011**, *5*, 1154–1164.
[63] V. Dua, S. P. Surwade, S. Ammu, S. R. Agnihotra, S. Jain, K. E. Roberts, S. Park, R. S. Ruoff, S. K. Manohar, *Angew. Chem.- Int. Edit.* **2010**, *49*, 2154–2157.

© 2014 WILEY-VCH Verlag GmbH & Co. KGaA, Weinheim